



# Optimization of synthesis parameters of mesoporous silica sol–gel thin films for application on 2024 aluminum alloy substrates



Isaline Recloux<sup>a,\*</sup>, Marc Debliquy<sup>a</sup>, Alexandra Baroni<sup>a</sup>, Yoann Paint<sup>b</sup>, Alex Lanzutti<sup>c</sup>, Lorenzo Fedrizzi<sup>c</sup>, Marie-Georges Olivier<sup>a</sup>

<sup>a</sup> Service de Science des Matériaux, Université de Mons, Place du Parc 23, 7000 Mons, Belgium

<sup>b</sup> Materia Nova asbl, Avenue Copernic 1, 7000 Mons, Belgium

<sup>c</sup> Dipartimento di Chimica, Fisica e Ambiente, Università di Udine, Via del Cotonificio 108, 33100 Udine, Italy

## ARTICLE INFO

### Article history:

Received 14 January 2013

Received in revised form 22 March 2013

Accepted 3 April 2013

Available online 16 April 2013

### Keywords:

Mesoporous film

Sol–gel

2024 aluminum

Template removal

Quartz crystal microbalance

Corrosion protection

## ABSTRACT

Silica mesoporous films were synthesized via Evaporation Induced Self-Assembly (EISA) using Pluronic P123 as templating agent and were applied on 2024 aluminum alloy for surface treatment applications. The removal of the P123 from the film required to convert the mesostructured film into a mesoporous film was particularly studied and optimized in order to be compatible with the use of an aluminum substrate. In this work, two different kinds of removal treatments were compared: calcination at high temperatures and UV/ozone treatment. Indeed, a minimum temperature of 275 °C has to be reached to completely remove the templating agent from the film. However, this treatment also leads to a decrease in mechanical properties of the aluminum substrate. In opposition, the removal by UV/ozone illumination allows getting mesoporous films at room temperature with important pore volume and high specific surface area without impacting mechanical properties of the aluminum. The effect of these treatments on mechanical properties of bare aluminum was followed by microhardness. The development of the porosity inside the film due to the elimination of the P123 was measured by combining analytical techniques (Fourier transform infrared spectroscopy FTIR, radio-frequency glow discharge optical emission spectroscopy RF-GDOES), electrochemical impedance spectroscopy (EIS) and adsorption porosimetry using a quartz crystal microbalance.

© 2013 Elsevier B.V. All rights reserved.

## 1. Introduction

Since the end of the 1990s, the synthesis of ordered mesoporous films and their use for different applications such as catalysis, drug delivery, sensors, low-k dielectrics and other electro-optical technologies have been reported in many papers [1–8]. These materials are obtained by using surfactant molecules, which act as templates during the synthesis of the sol–gel film, through the evaporation induced self-assembly (EISA) process. The transformation of the mesostructured film into mesoporous film is then achieved by eliminating the templating agent from the sol–gel matrix. The attractiveness of these films is mainly due to their ordered nanometric porosity (2–50 nm) and to their high specific surface area. Furthermore, the flexibility of the synthesis process allows getting

film properties adapted for each application. Intensive scientific efforts have been devoted to understand the influence of synthesis [4–6] and dip-coating [6–8] parameters on mesophase formation and to understand mechanisms of EISA process [5,8]. Films with controlled pore size, orientation and connectivity are now commonly obtained.

The removal of the templating agent is an important step just like the synthesis to obtain films of controlled morphology. It was already reported that the drying method could modify the mesostructure and consequently the accessibility to mesopores [9]. A thermal treatment with a slow heating rate up to a plateau temperature (around 400 °C) in air is generally achieved to transform micelles into mesopores. Alternative treatments, such as solvent extraction [10], supercritical fluid extraction [11] or UV/ozone [12], were also developed for applications which do not match with thermal treatment.

In recent years, a new application of mesoporous coatings has emerged in the field of anticorrosive protective coatings [13,14]. This technology was inspired by other applications using mesoporous films as carrier materials for prolonged or even controlled release of active substances (for example, in drug delivery). The approach consists in employing mesopores to host corrosion

\* Corresponding author. Tel.: +32 065 374488; fax: +32 065 374416.

E-mail addresses: [isaline.recloux@umons.ac.be](mailto:isaline.recloux@umons.ac.be) (I. Recloux), [marc.debliquy@umons.ac.be](mailto:marc.debliquy@umons.ac.be) (M. Debliquy), [alexandra.baroni@umons.ac.be](mailto:alexandra.baroni@umons.ac.be) (A. Baroni), [yoann.paint@materianova.be](mailto:yoann.paint@materianova.be) (Y. Paint), [alex.lanzutti@uniud.it](mailto:alex.lanzutti@uniud.it) (A. Lanzutti), [lorenzo.fedrizzi@uniud.it](mailto:lorenzo.fedrizzi@uniud.it) (L. Fedrizzi), [marjorie.olivier@umons.ac.be](mailto:marjorie.olivier@umons.ac.be) (M.-G. Olivier).

inhibitors and to obtain a self-healing coating to replace chromates based surface treatments which are very carcinogenic. The term “self-healing” here means a partial recovery of the initial properties of the coating after destructive action of the external environment [15].

For this application, mesoporous films are then applied on metallic substrates and more especially on 2024 aluminum which is particularly used in the aeronautical field due to its good strength to weight and cost ratio. For aircraft construction, one of the hardening treatments of 2024 aluminum (T6) consists in solution heat treating, quenching and peak aging at 177 °C for 4 h. However, it is well known that this type of aluminum loses its mechanical properties [16], such as tensile and yield stresses (Fig. 1), and develops an oxide layer on the surface when heated afterwards at a temperature higher than 177 °C. So, a particular attention has then to be paid for the removal of the templating agent from the film. Especially, a calcination process at high temperature could damage the metal.

In this work, silica mesostructured films have been synthesized through EISA process using Pluronic P123. A heating treatment in parallel with a UV/ozone process have been investigated to eliminate the templating agent and to obtain mesoporosity. The influence of the removal treatment on the porous structure and on the interface sol–gel/aluminum has been systematically studied. The goal was to control the removal of the P123 from the film to obtain an important open porosity and consequently an important volume for inhibitive molecules, without affecting the mechanical properties of 2024 aluminum. The effects of the heating or UV/ozone treatments on the mechanical properties of aluminum were studied by micro indentation and compared. Fourier transform infrared spectroscopy (FTIR) and radio–frequency glow discharge optical emission spectroscopy (RF-GDOES) have been used in combination to follow the chemical composition of the film with thermal and UV/ozone treatments. Electrochemical impedance spectroscopy (EIS) has also been used to detect the elimination of P123 and the formation of mesopores. Pore size distribution of films has been measured for each condition of removal by means of adsorption porosimetry using a quartz crystal microbalance. Moreover, the necessary interconnectivity of the pores was studied.

## 2. Materials and methods

### 2.1. Materials

The precursor solution was prepared by mixing absolute ethanol (Merck), structure-directing agent (Pluronic P123 (PEO)<sub>20</sub>-(PPO)<sub>70</sub>-(PEO)<sub>20</sub> from Sigma–Aldrich), tetraethylorthosilicate TEOS (Merck) and concentrated hydrochloric acid (Baker, 36 wt.%), used as received. In molar ratio, the composition was 1 TEOS: 0.005 P123: 6 H<sub>2</sub>O: 0.001 HCl: 9 EtOH. The quantity of water was chosen in order to promote hydrolysis of the alkoxide species and the pH value was set at 4 in order to slow down condensation reactions. The sol was left to react under stirring for 30 min at room temperature.

Mesostructured silica films were deposited by dip-coating at 70%RH/25 °C, with a withdrawal rate of 60 mm min<sup>-1</sup>. After dip-coating, the films were maintained in the deposition chamber in the same conditions of temperature and high humidity for 24 h. Working in a wet environment (>50%RH) promotes the periodic organization of micelles under mesophases inside the film [17]. The stabilization of the mesostructure is then achieved by drying films at 150 °C in air for 30 min on a thermalized plate.

The last step of the synthesis consists in removing the templating agent from the film and to transform mesophases into mesoporous network. In this work, two different ways were used

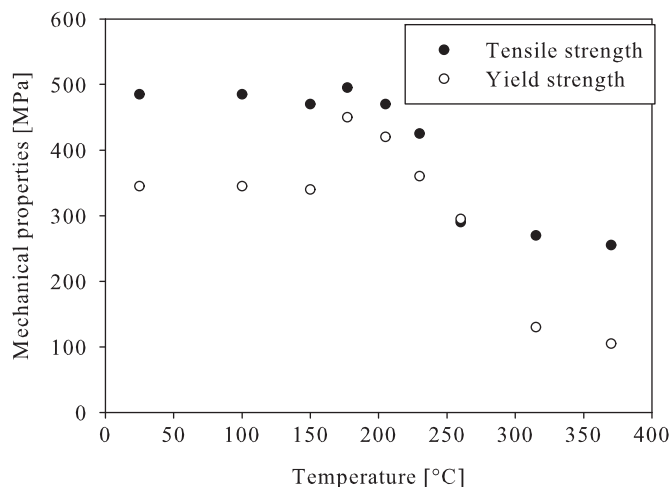


Fig. 1. Mechanical properties at room temperature of 2024-T3 aluminum after heating at indicated temperature for 10 h.

to remove the Pluronic P123: a thermal treatment at high temperature or a treatment under UV/ozone. The calcination treatment was performed in a furnace under air during 4 h with a temperature slope of 1 °C/min. Different maximal temperatures were tested in a range between 150 °C and 350 °C in order to determine the minimal temperature allowing the P123 removal. UV/ozone treatment was achieved by using a UV-ozone cabinet (PR-100 from AppliTek) for 24 h. The lamp spectrum contains two wavelengths at 185 nm and 254 nm which respectively forms ozone (about 50 ppm) and dissociates it in order to initiate the oxidization of organic substances.

### 2.2. Methods

Microhardness testing was performed on the matrix of bare 2024 aluminum (provided by Sonaca company, initially in T3 state: solution heat treated and then cold worked) to study the impact of removal treatment on mechanical properties of the substrate. The given values are the average of ten measurements taken at different places on the substrate. Tests were performed with a 136° Vickers diamond pyramid indent (nanoindenter M400 – Leco France) at 100 g load.

For the different characterizations of the films mentioned below, polished silicon substrates (Winfab Belgium), previously oxidized in a furnace, were used.

The thickness of mesoporous films was determined by ellipsometric measurements on a multiskop (Optrel GBR, Germany) with a 632.8 nm He–Ne laser beam as the light source. The data were evaluated and simulated by the program Elli. The morphology of mesoporous films was observed with a Philips CM200 TEM, equipped with a tungsten filament. The acceleration voltage was set at 120 kV. In that case, the films were scratched off the substrate, dispersed in ethanol and placed on copper grids covered with carbon micromesh coating.

Complementary techniques were used to detect the removal of Pluronic P123 from the film.

Thermogravimetric analyses (TGA) were achieved with a TGA Q50 apparatus (T.A. Instruments) under air flow at a temperature scan of 2 °C/min until 600 °C.

Composition profiles were recorded in depth by RF-GDOES using a Horiba-Jobin Yvon GD profiler (4 mm diameter anode, 28 acquiring channels polychromator, 13.6 MHz RF-generator and Quantum XP software). The Ar pressure was set at 650 Pa and the source power was applied at 40 W for the analysis. The instrument was equipped with a 0.5 m Paschen Runge polychromator with nitrogen purged optical path. For the calibration of the analysis method, 25

CRMs (certified reference materials) and SUSs (setting up samples) were used.

FTIR spectra (average of 10 scans) were recorded on a Perkin-Elmer 2000 spectrophotometer with a resolution of  $4\text{ cm}^{-1}$  in the range of  $4000\text{--}370\text{ cm}^{-1}$ .

EIS measurements were used for two different purposes. Bare aluminum was firstly characterized in order to highlight the formation of an oxide layer on the surface due to the removal treatment. Aluminum coated with sol-gel was secondly analyzed to confirm the presence of a porous layer. A three-electrode cell consisting of a silver chloride reference electrode, a platinum foil counter electrode and the sample as the working electrode (exposed area of  $4.5\text{ cm}^2$ ) were used. The cell was placed in a Faraday cage to avoid electromagnetic interferences.  $0.1\text{ M Na}_2\text{SO}_4$  was used as electrolyte to characterize layers without inducing corrosion processes on the metallic substrate. Measurements were performed after one hour of immersion using an AMETEK Parstat 2273 computer controlled using Powersuite® software. The frequency was ranged from  $100\text{ kHz}$  to  $10\text{ mHz}$  using a  $10\text{ mV RMS}$  amplitude signal voltage vs. open circuit potential. Impedance plots were fitted with different RC equivalent circuits by using ZsimpWin® software and by replacing pure capacitances by constant-phase elements (CPE) to describe the frequency dependence of non ideal capacitive behavior and to improve the goodness of fitting. A constant phase element can be written as in Eq. (1).

$$Q_{\text{CPE}} = \frac{1}{(j\omega)^n \cdot C} \quad (1)$$

when  $n$  tends to 1, the CPE corresponds to a pure capacitance and in the opposite, a  $n$  value close to 0 indicates a resistive behavior. The error of the fitting, expressed by chi square  $\chi^2$  was lower than 0.01. The quality of the fit is expressed by this parameter. The lower the value of  $\chi^2$ , the better the fitting of the calculated data to the experimentally measured.

For these characterizations (FTIR, RF-GDOES and EIS), mesostructured films were dip coated on polished 1050 aluminum substrates (provided by Sonaca company). For EIS measurements, the use of polished 1050 aluminum allows focusing on oxide layer and sol-gel layer properties due to the low reactivity of this kind of aluminum. In that case, no interfering corrosion current is expected. For FTIR measurements, polished aluminum was necessary to operate in reflection mode. More generally, the use of polished 1050 aluminum, which is more stable, in place of 2024 aluminum allows carrying out measurements in ideal conditions. In order to promote adhesion of the sol-gel, aluminum was degreased in an alkaline bath (TURCO 4215-NC-LT – pH 9) during 20 min at  $50^\circ\text{C}$ . This pretreatment promotes the formation of OH groups at the aluminum surface which ensure a better uniformity and adhesion of the film [18]. It is also worth noting that due to the presence of the surfactant, the sol perfectly wets the substrate surface.

Due to the limited quantity of matter available from this kind of thin films, it is very difficult to obtain porosity from liquid nitrogen adsorption-desorption at  $77\text{ K}$ , which is more adapted for bulk materials and powders. For this reason, another adsorption porosimetry method, developed by Baklanov [19], was used to obtain porous characteristics of the film. The technique is based on the use of a quartz crystal microbalance (QCM) to measure vapor adsorption and desorption quantities for different partial pressures in gas. QCM is indeed able to accurately detect very tiny mass changes (about  $10^{-8}\text{ g/Hz}$ ) by measuring variations of frequency.

For this measurement, mesoporous films are dip coated on the surface of an AT-cut quartz resonator ( $6\text{ MHz}$ ) and placed in a closed chamber in which water vapor partial pressure can be controlled from 0 up to the saturated vapor pressure  $P_0$  at room temperature. Fig. 2 depicts the experimental set up.

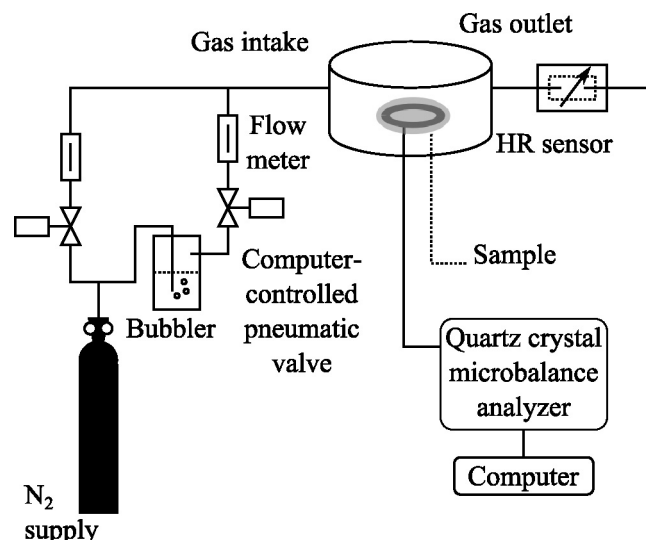


Fig. 2. Schematic diagram of the instrumentation for measuring adsorption porosimetry.

Unlike Baklanov's work, a mix of water vapor and nitrogen was used as adsorbate and pressure was measured in the chamber with a humidity sensor. Before each test, samples were exposed to dry air for 90 min, to ensure that water was completely desorbed. The speed at which water partial pressure is changed was chosen in order to be sure that adsorption/desorption equilibrium is reached for each weight measurement.

Given that the analysis is directly achieved on the supported film, the measurement is adapted for the study of thin films. Moreover, the technique is non destructive and can be carried out at room temperature. In comparison with the environmental ellipsometric porosimetry [20], this method, which is based on mass measurements, also allows to avoid the use of indirect determinations based on mathematic models.

Finally, contact angle measurements were carried out with a GDX digidrop goniometer with a video camera system and the Visiodrop software. Teflon-coated needles were used to dispense water. The advancing contact angles of water were measured after deposited  $5.6\text{ }\mu\text{l}$  on the sample surface. The reported data are the average of contact angles obtained from ten drops measured on both sides.

### 3. Results and discussion

#### 3.1. Influence of the removal treatment on bare aluminum substrates

##### 3.1.1. Formation of an oxide layer

It is well known that heating aluminum at high temperature induces an increase of the  $\text{Al}_2\text{O}_3$  film thickness [21]. The UV/ozone treatment should also lead to the same phenomenon due to the strong oxidizing ability of  $\text{O}_3$  (superior to  $\text{O}_2$ ). Alumina is an oxide which is stable, continuous and adherent. The presence of this passivation film, as a barrier against aggressive species, provides then superior corrosion resistance. The formation of this oxide was put in evidence by EIS achieved on bare 1050 polished aluminum substrates which were submitted to the different removal treatments. Fig. 3 shows the EIS spectra of bare aluminum treated at different temperatures (between  $150^\circ\text{C}$  and  $350^\circ\text{C}$ ) and under UV/ $\text{O}_3$ . Only phase bode plot allows observing a difference. At low frequencies ( $10^{-2}\text{ Hz}$ ), the aluminum treated at higher temperatures or exposed under UV/ozone for 24 h present an almost pure capacitive behavior while reference bare aluminum (without treatment) and

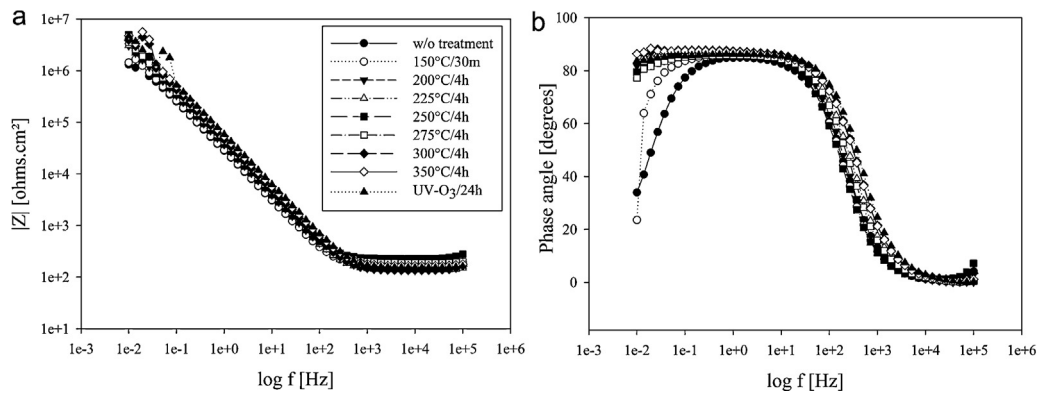


**Fig. 3.** Bode plots in modulus (a) and in phase angle (b) of bare polished 1050 aluminum treated at different temperatures and under UV/ozone after 1 h of immersion in 0.1 M Na<sub>2</sub>SO<sub>4</sub> solution.

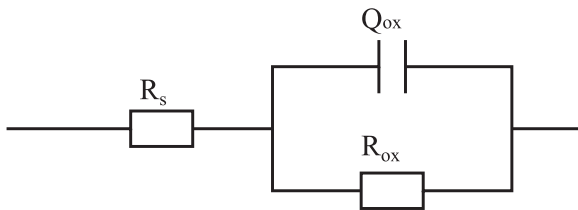


**Fig. 4.** Electrical equivalent circuit used to model the impedance behavior of bare aluminum.

the aluminum treated at 150 °C during 30 min present a resistive component.

The spectra were also fitted with the electrical equivalent circuit shown in Fig. 4. This model has been widely accepted in the literature for natural aluminum oxide layers [22].  $R_s$  and  $R_{ox}$  are respectively electrolyte and oxide layer resistances and  $Q_{ox}$  is the oxide layer capacitance.

The results of the fittings are shown in Fig. 5.

The resistance of the alumina film is around ten times higher when a treatment is achieved and even fifty times higher when temperature of 350 °C is reached. Treatment under UV/ozone also gives a reinforcement of the passivation film with a resistance similar to the resistance obtained at intermediate temperatures (around 225 °C). Capacitance values also show the same tendency, with a first decrease when a treatment is applied and a second decrease when higher temperatures are reached. It is worth noting that  $n_{ox}$  is in the range 0.96–1.00, meaning that the system can be described

almost by a pure capacitance. Capacitance values can be used to calculate the thickness of the oxide using Eq. (2).

$$C = \frac{\varepsilon \cdot \varepsilon_0 \cdot A}{d} \quad (2)$$

where  $C$  is the capacitance,  $\varepsilon$  is the dielectric constant,  $\varepsilon_0 = 8.85 \times 10^{-12}$  F/m,  $A$  is the area of the sample and  $d$  is the thickness of the oxide. These values, reported in the Fig. 6, may differ from the reality as an assumption has to be taken for the value of  $\varepsilon$  (fixed at 10 in this work in agreement with the literature [23]).

The thickness of the oxide layer increases with the temperature of the thermal treatment, consistent with the trend observed for capacitances. However, in the case of UV/O<sub>3</sub>, the value of the thickness is surprisingly high compared to the relative resistance which is quite low, suggesting that the passivation layer is less dense than for films induced by treatment at high temperature.

### 3.1.2. Mechanical properties

In addition with the development of an oxide layer on the surface, the treatment achieved to remove the templating agent mainly modifies mechanical properties of aluminum. While the effect of elevated temperatures on 2024 aluminum alloy is already known [16], the influence of a UV/O<sub>3</sub> treatment on mechanical properties of this alloy has never been studied. Vickers microhardness measurements were consequently achieved to compare both treatments: thermal and under UV/O<sub>3</sub>.

As seen in Fig. 7, an increase of the removal treatment temperature for a constant period of time (4 h) reduces the hardness. This variation in mechanical properties is explained by a

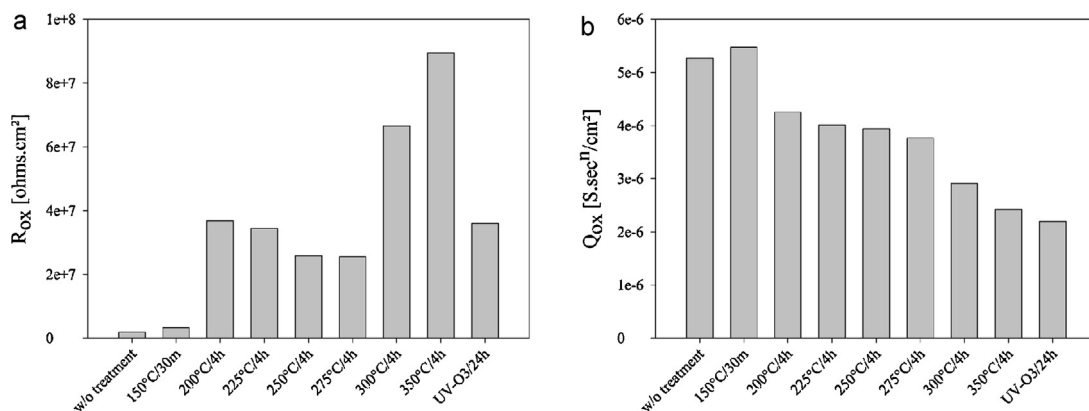


**Fig. 5.** Resistance  $R_{ox}$  (a) and capacitance  $Q_{ox}$  (b) of oxide layer of bare polished 1050 aluminum treated at different temperatures and under UV/ozone after one hour of immersion in 0.1 M Na<sub>2</sub>SO<sub>4</sub>.

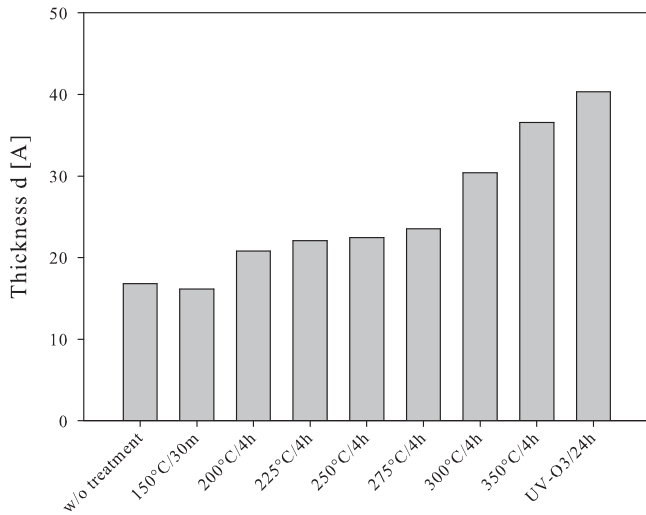


**Fig. 6.** Oxide layer thicknesses of aluminum treated at high temperatures and under UV/ozone.

transformation of nanoscale precipitates, which are introduced into the microstructure during the aging step. According to the Al–Cu phase diagram, 2024 aluminum is suitable for age hardening as the solubility of the copper is high at the eutectic temperature and decreases rapidly at lower temperatures. In fact, the heating treatment of aluminum is comprised of three main stages which are solution heat treatment, quenching and aging. The first step is achieved at temperature higher than eutectic temperature and aims at dissolving the copper elements into the matrix. A supersaturated solid solution of copper in aluminum is obtained when room temperature is obtained after quenching. The last stage, which is called aging, consists in controlling the decomposition of the supersaturated solid solution to form a fine dispersion of precipitates and finally an equilibrium structure. This transformation occurs at any temperature below the solvus temperature, even at room temperature.

For 2024 aluminum, different intermediate stages occur before reaching the equilibrium compound  $\text{Al}_2\text{CuMg}$ :

Supersaturated solid solution  $\alpha \rightarrow$  Guinier–Preston–Bagaryatsky (GPB) zones  $\rightarrow \theta'' \rightarrow \theta' \rightarrow \theta (\text{Al}_2\text{CuMg})$ .

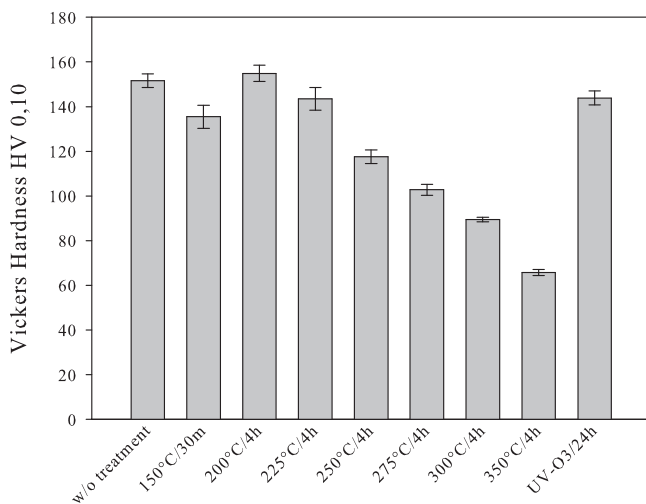


**Fig. 7.** Influence of different (thermal and UV/O<sub>3</sub>) treatments on hardness of 2024 aluminum.

Diffusion during aging results in localized concentrations of copper atoms on specific planes of aluminum lattice which are called GP zones. Coherent intermediate phases  $\theta''$  are then formed from these GP zones which provide nucleation sites. The aluminum atoms round this plane distort to accommodate this new phase leading to coherency strains. As precipitates become larger, formation of dislocations occur at the interface with the matrix and semi-coherent  $\theta'$  precipitates are formed. Upon sufficient aging, the equilibrium phase is finally formed.  $\text{Al}_2\text{CuMg}$  has a different crystal structure from the matrix and coherency strains are completely eliminated.

Depending on the time and temperature, the aging process results in formation of one of these stages which offer different hardenings. The phase which is the most hardening is the  $\theta'$  phase (semi-coherent). However, once the critical temperature or aging time are exceeded,  $\theta$  precipitates begin to be formed and hardness drastically decreases due to the complete incoherence of  $\theta$  phase with the aluminum matrix [24].

In opposition, the UV/O<sub>3</sub> treatment does not seem to impact mechanical properties. The hardness measured after the treatment is similar to the hardness obtained without any treatment. The UV/ozone removal treatment could then be investigated to decompose the templating agent without modifying mechanical properties of the alloy.

### 3.2. Synthesis of mesoporous films and morphology characterization

Silica mesostructured films were produced through the EISA process using P123 from Pluronic family as templating agent. Films obtained by dip coating on silicon substrates for TEM imaging uniformly cover the surface and present optical quality. Based on the uniform coloration of the surface, the thickness seems to be homogeneous. Ellipsometric measurements determine that the thickness is about 280 nm for a mesoporous film calcinated at 350 °C during 4 h (with a refractive index set at 1.37 according to literature [25]).

The choice of P123 as structuring-agent is due to multiple reasons:

1. From the literature [4], it was already shown that cubic mesostructure can be obtained using P123 in suitable quantity in the sol (based on phase binary diagram of P123 in water). For applications such as hosting, cubic mesophase is crucial to obtain pore accessibility and through-film pore connectivity [26]. If hexagonal structure is synthesized, pore channels are aligned within the substrate plane and do not provide easy accessibility to corrosion inhibitors.
2. Uniform pore size about 5–7 nm is obtained with P123 and this dimension is compatible with the average diameter of corrosion inhibitor molecules (for example, benzotriazole which is a well known inhibitor for aluminum has an average diameter of 0.6 nm). The incorporation of active molecules inside the mesopores could then be considered in a next step.
3. P123 belongs to the Pluronic family and is a non ionic block copolymer ((PEO)<sub>20</sub>-(PPO)<sub>70</sub>-(PEO)<sub>20</sub>). In opposition with other ionic templating agents which can be used to structure the film, interactions, created between silica matrix and surfactant, are hydrogen bonds which are more easily cleaved than electrostatic bonds. The removal of surfactant from the film is then enhanced when P123 is used.

The morphology of the films synthesized in this work was characterized by TEM. In order to detect the modifications induced by the removal treatment on the structure, different kinds of films were imaged: (a) a mesostructured film stabilized at 150 °C for 30 min but still containing P123; (b) a mesoporous film obtained

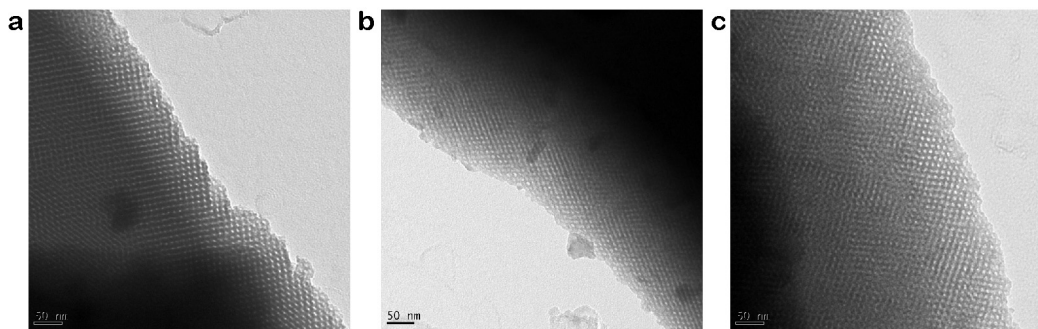


**Fig. 8.** TEM pictures of a mesostructured film (a), a mesoporous film after thermal treatment at 350 °C for 4 h (b) and a mesoporous film after UV/O<sub>3</sub> treatment for 24 h (c).

after thermal treatment at 350 °C for 4 h and finally (c) a mesoporous film obtained after UV/O<sub>3</sub> treatment for 24 h.

All the TEM images present similar cubic structure with well-ordered pores, as expected from the literature [4]. For Fig. 8(a), the contrast in image is due to the difference between inorganic and organic phases which respectively constitute the silica matrix and micelles of P123. In opposition, for Fig. 8(b) and (c), the contrast should be due to difference between silica matrix and void if the extraction of P123 is successful. This fact shall be checked in a next section with adsorption porosimetry. However, assuming that P123 is well decomposed, the film structure is still present after removal treatment showing that the silica matrix does not collapse when P123 leaves the film. Pore sizes are comprised between 5 and 7 nm, which is in good agreement with previous works [4].

### 3.3. Removal of P123 templating agent from the film and transformation of micelles into mesopores

As said previously, a special treatment must be applied to the films to degrade P123 inside the film and to transform micelles into mesopores. This treatment is particularly important for our application as the mechanical properties of 2024 aluminum are very sensitive to elevated temperatures. Thermogravimetric analysis (TGA) was firstly used to determine if the P123 is degraded in the same way when used alone or in the silica film. For this purpose, analyses were recorded firstly on pure P123 and then on a mesostructured gel containing P123. The mesostructured gel was obtained by leaving the previously described sol without stirring until a complete cross-linking of the silica network (around two months). Fig. 9 shows the weight loss (a) and the derivative curves (b) of pure P123 and mesostructured gel containing P123.

When used alone, Pluronic P123 is decomposed at 177 °C. In opposition, when P123 is incorporated in the sol–gel mesostructured film, a slight shift is observed toward higher temperature

with a maximum decomposition rate at 200 °C. The decomposition also seems to extend over a larger temperature range. Furthermore, a second peak is observed at 37 °C and is relative to the residual ethanol in the film. This result shows that the copolymer included in the sol–gel bulk matrix needs higher temperatures to be completely eliminated. In fact, when P123 is used as templating agent in the sol, hydrogen bonds are created between copolymer and silica precursors. The creation of this hybrid interface between organic and inorganic species is a fundamental requisite for the formation of micelles in the film [27] but also implies that more energy is needed to remove P123 from the matrix.

In opposition with TGA analyses, Rf-GDOES measurements can be applied directly on thin films and allow obtaining chemical composition in relation with layer depth. Mesostructured films (treated at different temperatures) were analyzed in conjunction with classical sol–gel films that do not contain P123 in order to determine if the technique is sufficiently sensitive to trace the presence of the templating agent. The carbon signal obtained at a constant thickness of 0.08 μm for each film is reported in the Fig. 10 according to the temperature of the thermal treatment. This thickness was chosen in order to avoid the carbon pollution occurring at the surface of the sample. As expected, a difference in carbon content is observed between classical films and mesostructured films treated at 150 °C during 30 min, due to the presence of P123.

For classical sol–gel films, the carbon content is very low and constant with the heat treatment. In opposition, for mesostructured films, the quantity of carbon continuously decreases until 275 °C, in agreement with the removal of P123 from the film. For this temperature, the carbon signal is similar to the value obtained for a classical sol–gel film, meaning that the P123 is completely eliminated from the film. As previously observed with TGA measurements, more elevated temperatures (minimum temperature of 275 °C) appear to be required to decompose P123 when the latter is linked to silica inorganic species. Nevertheless, as seen previously, this

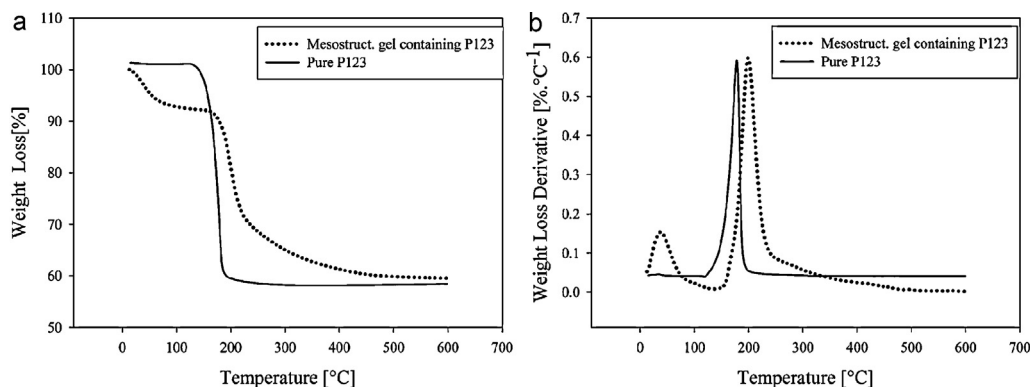


**Fig. 9.** Thermogravimetric analyses of pure P123 and of mesostructured gel containing P123 with (a) the weight loss and (b) the derivative curves.

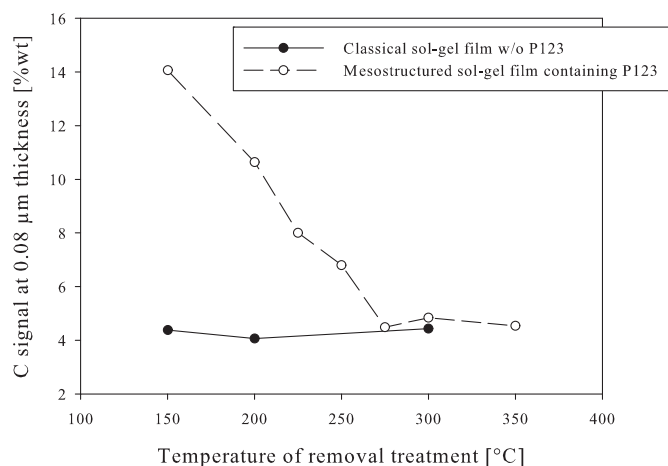


**Fig. 10.** Evolution of carbon signal (at a fixed thickness) according to removal temperature for classical sol-gel films that do not contain P123 and mesostructured sol-gel films.

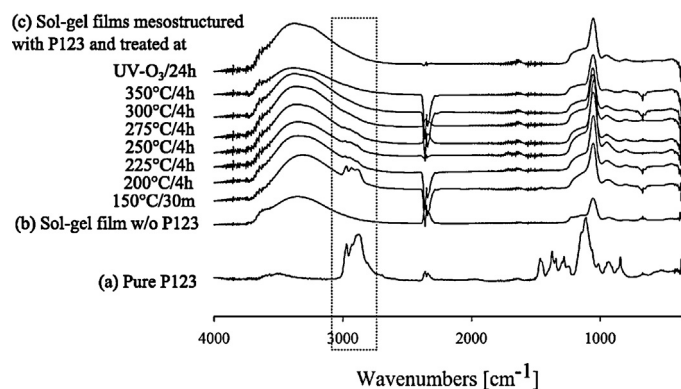


**Fig. 11.** FTIR absorption spectra, in the range, 4000–370  $\text{cm}^{-1}$  of (a) pure P123, (b) classical sol-gel film w/o P123 and (c) silica mesostructured films treated at different temperatures and under UV/O<sub>3</sub>.

temperature is too high and induces a drop of about 30% in mechanical properties of 2024 aluminum.

FTIR measurements were consequently achieved to evaluate the efficiency of the alternative UV/ozone treatment to remove P123. Fig. 11 shows the FTIR absorption spectra in the range 4000–370  $\text{cm}^{-1}$  for (a) pure P123, (b) classical sol-gel film which does not contain P123 and (c) mesostructured films treated at different temperatures and under UV/O<sub>3</sub>.

The main peaks observed for pure P123 are assigned and reported in Table 1.

The absorption band observed in the range of 3000–2800  $\text{cm}^{-1}$  for mesostructured film stabilized at 150 °C for 30 min is due to absorption of Pluronic P123 methyl groups still present in the film. For classical non mesostructured sol-gel films (b), these peaks are missing, demonstrating that this absorption band can be taken as a signature of the presence of the block copolymer within the film. As already confirmed by RF-GDOES analyses, these peaks

**Table 1**  
Assignment of important bands for FTIR spectra of P123.

Wavenumbers [ $\text{cm}^{-1}$ ]	Assignment
3000–2840	CH stretching
2962	Asymmetrical CH <sub>3</sub> stretching
2872	Symmetrical CH <sub>3</sub> stretching
1400	CH <sub>3</sub> bending
1150–1085	Asymmetrical C—O—C stretching

also disappeared when a temperature of 275 °C is reached for mesostructured films, due to the complete removal of P123. Aside from the temperature effect, detection of P123 removal from the film by ozone treatment was also possible. After UV/O<sub>3</sub> treatment, the C—H peaks are no longer observed whereas peaks relative to Si—OH (960  $\text{cm}^{-1}$ ) and to Si—O—Si (1100–1000  $\text{cm}^{-1}$ ) are still detected, meaning that the sol-gel matrix is not destroyed by the treatment. The elimination of organic molecules and the transformation of mesostructured film in mesoporous material are then possible at room temperature. Optimization of the duration under UV/O<sub>3</sub> treatment should be achieved in a further work.

While FTIR and RF-GDOES measurements are based on the chemical composition of the film, the monitor of the removal of the P123 from the film is also possible by EIS measurements. Indeed, if the film presents an open and interconnected porosity, the metal should be exposed to the solution that can penetrate the film. We should then observe a low frequency behavior close to that of the metal without treatment. This can be evidenced by the EIS measurements presented in Fig. 12.

From Bode plots in modulus (Fig. 12(a)) and in phase angle (Fig. 12(b)), it can be seen that the removal treatment induces a modification. A reference relative to non coated bare aluminum is also added. As expected, all samples, except the mesostructured film stabilized at 150 °C/30 min, present a relaxation time constant in the range of low and medium frequencies (around 2 Hz) which can be attributed to the oxide film present on the aluminum surface and show a behavior very close to that of the bare metal. The film without removal of the template presents an additional barrier against electrolyte represented by the second relaxation time constant at a frequency about  $2.5 \cdot 10^4$  Hz which can be related, as already seen in literature [22], to the sol-gel layer present on the aluminum surface. As soon as the thermal treatment at 275 °C or the UV/O<sub>3</sub> treatment is applied, this second time constant disappears due to the weakening of the barrier properties of the film. After these removal processes, P123 is completely decomposed, as already demonstrated by FTIR and Rf-GDOES, and the impedance behavior moves toward that of bare aluminum with the apparition of a resistive contribution at low frequencies. It is then possible to conclude that pores are interconnected and form pathways open on the aluminum surface. By comparing these results with EIS measurements obtained on bare aluminum and based on low-frequency behavior, it is also possible to see that oxidization of the substrate does not seem to appear when the aluminum is coated by the sol-gel film. The time constant relative to oxide layer seems not to be reinforced by the removal treatment at 275 °C or under UV/O<sub>3</sub>.

### 3.4. Determination of pore characteristics of the film

The determination of film characteristics, such as the specific surface area or the pore volume, is particularly important for its application as nanocontainer for active molecules. The effect of the removal treatment on porosity of the sol-gel film was thus also studied by adsorption porosimetry to obtain quantitative information on the pore network.

Fig. 13(a) and (b) depict results obtained during water adsorption and desorption isotherms respectively for a blank QCM and for a QCM covered with a mesoporous film (calcined at 350 °C for 4 h). The y axis “frequency difference” corresponds to the difference between the measured frequency at a certain pressure and the frequency of the dry film at the initial stage (of the dry QCM for case (b)). This response is consequently due to the adsorption or desorption of water from the film or from the surface of the QCM. Variations are larger for the mesoporous film due to the possible condensation of water inside the mesopores. In opposition, for bare QCM, water can only adsorb on the surface.

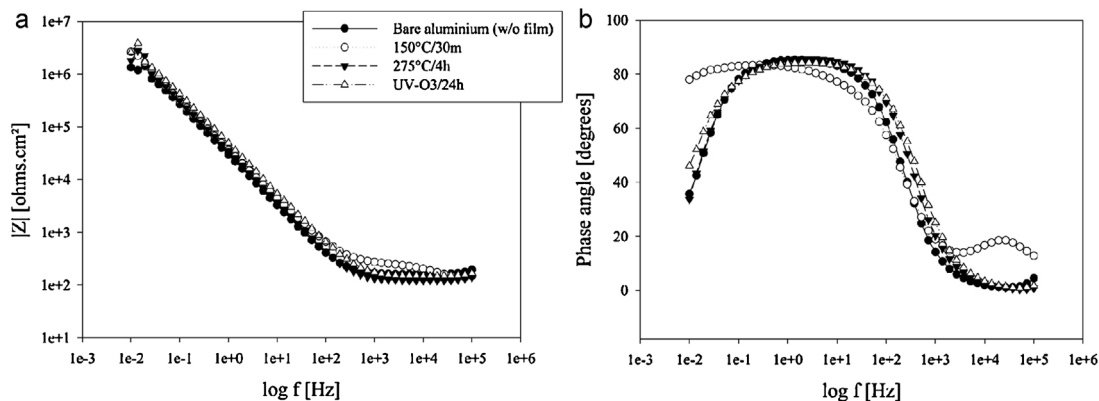


Fig. 12. Bode plots in modulus (a) and in phase angle (b) of mesostructured films submitted to different removal treatments after one hour of immersion in 0.1 M  $\text{Na}_2\text{SO}_4$  solution.

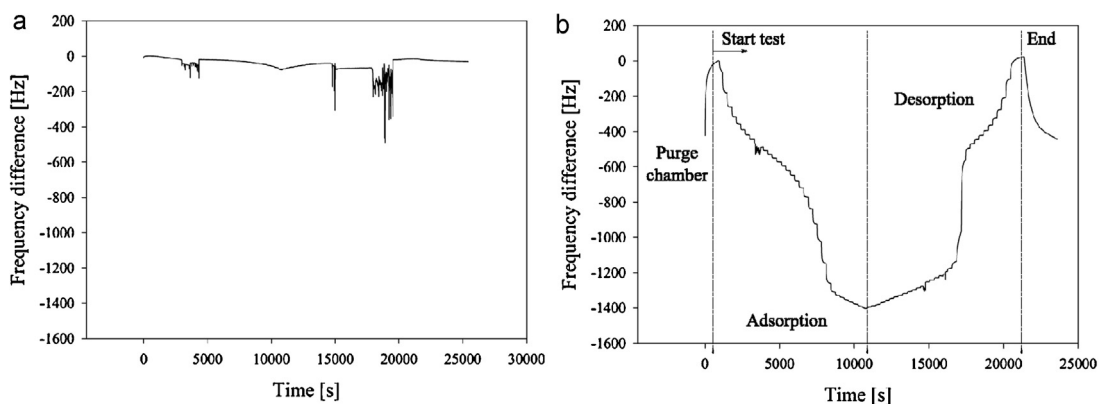


Fig. 13. Typical frequency response curves for water adsorption and desorption isotherms on bare QCM (a) and QCM coated with a mesoporous sol-gel ( $350^\circ\text{C}/4\text{h}$ ) (b).

Frequency variations of the quartz crystal resonator can be converted into mass uptake  $\Delta m$ , using the Sauerbrey equation [28] (3).

$$\Delta f = \frac{-2 \cdot f_q^2 \cdot \Delta m}{(\mu_q \cdot \rho_q)^{1/2} \cdot A} \quad (3)$$

where  $f_q$  is the resonant frequency of the quartz,  $\rho_q$  the quartz density,  $\mu_q$  the shear modulus of quartz and  $A$  the surface area between electrodes. In order to get the relative amount of adsorbed water vapor and to be able to compare isotherms of different films, the mass uptake was also divided by the mass of the film. Fig. 14 reports the dependence of this relative amount of gas on relative pressure in water for films calcined at different temperatures or treated under UV/ozone.

Two main behaviors are obtained according to the presence of mesopores. For mesostructured film stabilized at  $150^\circ\text{C}$  during 30 min, adsorption and desorption isotherms are superimposed. In this case, the P123 is still present in the porosity and the amount of adsorbed water is low. For the other films, a hysteresis loop appears due to the capillary condensation. As described in the Kelvin equation [20] (4), the adsorbate can indeed condense in the pores of an adsorbent even if the vapor pressure  $P$  is less than the equilibrium pressure of a flat liquid surface  $P_0$ .

$$RT \ln \left( \frac{P}{P_0} \right) = -2\gamma V_L \cos \theta \frac{1}{r_m} \quad (4)$$

with  $r_m$  is the curvature radius (close to the pore radius),  $\gamma$  is the liquid-air surface tension,  $V_L$  is the molar volume of the adsorbate after capillary condensation and  $\theta$ , the solid/liquid wetting angle. According to I.U.P.A.C. classification [29], this shape of adsorption

and desorption isotherms corresponds to the type IV which is typical of mesoporous adsorbents. The hysteresis loop is due to the curvature radius of the meniscus of the condensing liquid which is different for adsorption and desorption. The phenomenon can happen if pores present shape with two dimensions (presence of a neck) or if a swelling or shrinkage occurs during the adsorption/desorption cycle [30]. In this case, the increase and the decrease in relative mass uptake are very steep, demonstrating

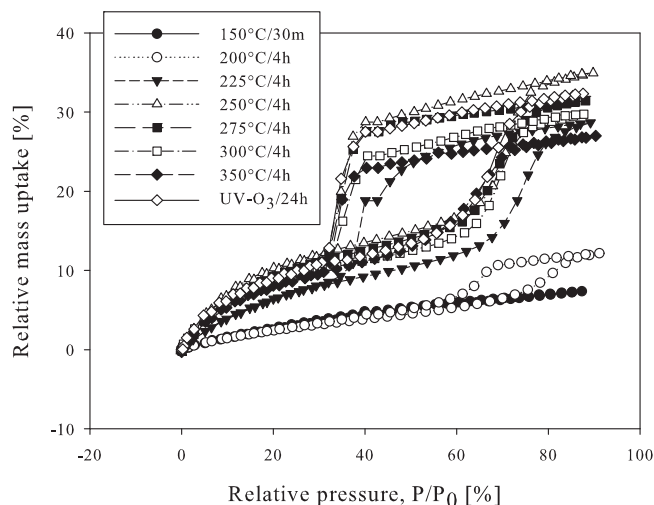


Fig. 14. Adsorption and desorption isotherms of water vapor on films calcined for 4 h at different temperatures or submitted to UV/ $\text{O}_3$  during 24 h.

**Table 2**  
Porous properties of films submitted to different removal treatments.

Removal treatment	Ratio of H <sub>2</sub> O adsorption [wt%]	Porosity, $\varepsilon$ [vol%]	Specific surface area [m <sup>2</sup> /g]	B.E.T. coefficient, $R^2$
150 °C/30 min	7.4	13.9	140	0.9438
200 °C/4 h	12.9	21.1	118	0.9870
225 °C/4 h	35.1	38.7	279	0.9950
250 °C/4 h	34.9	43.4	365	0.9914
275 °C/4 h	33.9	40.8	359	0.9920
300 °C/4 h	29.7	39.5	306	0.9973
350 °C/4 h	26.9	37.3	296	0.9941
UV-O <sub>3</sub> /24 h	32.3	41.6	325	0.9949

that pores present regular shape and dimensions and so that the mesostructure is well defined. For the mesostructured film treated at 200 °C during 4 h, the hysteresis appears but is shifted toward higher relative pressure and the relative mass uptake in water is less important. By combining this result with previous analyses, it is possible to conclude that P123 is not yet completely removed from the film at this temperature. The shift at higher pressure is explained by the presence of residual P123 inside the film which leads to an increase of the solid/liquid wetting angle  $\theta$  and consequently to an increase of the pressure at which liquid condensates according to Kelvin equation. For the film calcined at 200 °C during 4 h, the wetting angle was indeed  $72.8^\circ \pm 1.2^\circ$  while the mesoporous film calcined at 350 °C during 4 h presents a wetting angle of  $13.7^\circ \pm 1.4^\circ$ .

Table 2 reports the mass ratio obtained at the maximum value of pressure in water (close to the saturated vapor pressure) for each sample. These values correspond to the ratios of adsorbed mass of H<sub>2</sub>O to the amount of film deposited and already provide a good estimate of the ability of the film to host molecules. However, porosity is generally expressed in terms of volume. To calculate this porosity in ratio in volume,  $\Delta m_1$  and  $\Delta m_2$ , corresponding respectively to the mass of the dry film and to the mass of the wet film (at the highest pressure in water), were used.

$$\Delta m_1 = V_{\text{SiO}_2} \cdot \rho_{\text{SiO}_2} + V_{\text{air}} \cdot \rho_{\text{air}} \quad (5)$$

In Eq. (5),  $\rho_{\text{SiO}_2}$  was assumed to be equal to 2.2 g/cm<sup>3</sup> and the term  $V_{\text{air}} \cdot \rho_{\text{air}}$  was neglected due to the low density of air in comparison with silica.

$$\Delta m_2 = V_{\text{SiO}_2} \cdot \rho_{\text{SiO}_2} + V_{\text{H}_2\text{O}} \cdot \rho_{\text{H}_2\text{O}} \quad (6)$$

After capillary condensation process, water is assumed to be liquid inside the mesoporosity and  $\rho_{\text{H}_2\text{O}}$  is assumed to be equal to 1 g/cm<sup>3</sup> in equation (6). If all pores open at the surface are filled by water,  $V_{\text{H}_2\text{O}}$  corresponds to the opened pore volume of the film  $V_p$ .

By combining Eqs. (5) and (6), it is then possible to obtain the porosity in volume  $\varepsilon$  (Eq. (7)) which is also reported in Table 2 for each sample.

$$\varepsilon = \frac{V_p}{V_{\text{SiO}_2} + V_p} = \frac{1}{1 + (\Delta m_1/2, 2 \cdot (\Delta m_2 - \Delta m_1))} \quad (7)$$

The Brunauer–Emmet–Teller [31] (BET) method was also applied to the data obtained for water relative pressure between 0.05 and 0.3 to get the specific surface area of adsorption. Molecular cross-sectional area of 0.114 nm<sup>2</sup> was used for H<sub>2</sub>O. Table 2 summarizes the resulting specific surface area  $S_S$  according to removal treatment. The coefficient of determination  $R^2$  of the regression line of BET data was also added for each sample.

It is worth noting that a part of water molecules are adsorbed on the surface of the film as well as on uncovered area by the film of the gold electrodes and that the porosity is consequently slightly overestimated. Porosity obtained is in good agreement with the quantity of P123 added in the sol which is 30% in volume when only taking into account nonvolatile components of the solution. As soon as a temperature of 225 °C is reached, the film presents an interesting pore volume coupled with a high specific surface area. The film treated under UV/ozone during 24 h presents similar porous properties as the film calcined at 275 °C during 4 h, demonstrating the good efficiency of the process to oxidize P123 into gaseous products and to remove it from the porosity. The decrease in porosity observed from 250 °C could be due to a slight collapse of the silica walls due to thermal treatment.

The pore size distribution was also calculated using Kelvin equation and BJH (Barret, Joyner, Halenda) method for mesoporous films (calcined at 275 °C for 4 h and treated under UV/O<sub>3</sub> during 24 h). In this case, BJH was applied both to adsorption and desorption branches of the isotherm to compare results (Fig. 15).

Pore size distributions are similar for both removal treatments. Data collected from adsorption and desorption isotherms are

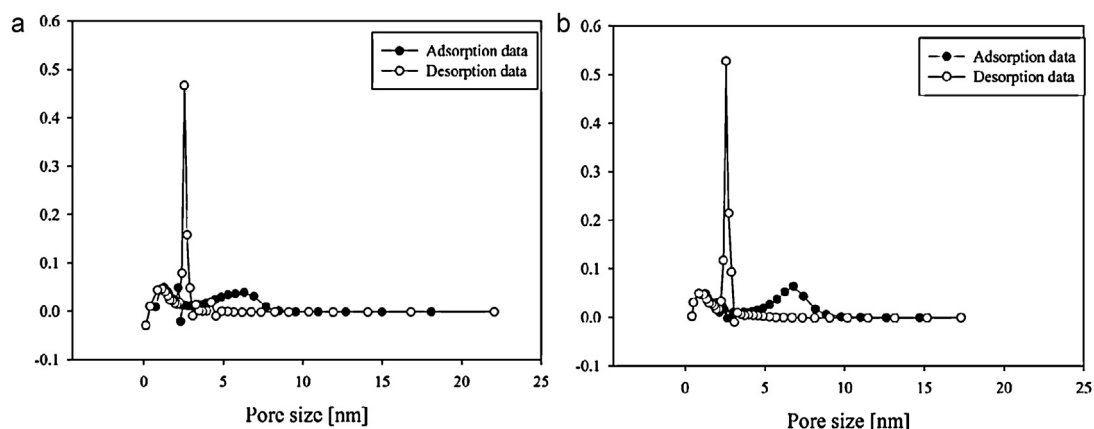


**Fig. 15.** Pore size distributions of mesoporous film calcined at 275 °C during 4 h (a) and mesoporous film treated under UV/ozone during 24 h obtained from adsorption and desorption isotherms (b).

**Table 3**  
Comparison of pore diameters obtained by different ways for films treated at 275 °C during 4 h and films treated under UV/ozone.

Removal treatment	$D_{\text{pore}}$ (BJH <sub>ads</sub> ) [nm]	$D_{\text{pore}}$ (BJH <sub>des</sub> ) [nm]	$D_{\text{pore}}$ ( $d = 6 \cdot V/S$ ) [nm]	$D_{\text{pore}}$ (TEM) [nm]
275 °C/4 h	6.3	2.4	5.5	6
UV-O <sub>3</sub> /24 h	6.8	2.6	6.0	6

different. The pore size seems to be smaller when data are collected from desorption isotherm. This fact can be due to the presence of the so-called pore restrictions or necks which are in fact the openings joining one pore to another pore (where the desorption begins). In opposition, the adsorption firstly occurs inside the mesopore, providing a value closer to the actual pore diameter.

A second method which is based on simple geometric assumptions was also used to estimate the pore size. By assuming that pores are quite spherical (in view of TEM results), an average diameter can also be determined by combining both pore volume and surface developed by the film using Eq. (8).

$$d = \frac{6 \cdot V}{S} \quad (8)$$

Table 3 reports the comparison of pore size obtained by BJH method (adsorption and desorption), by geometric method and by TEM imaging. As previously suggested, data collected from desorption isotherm seem to be less suitable to estimate pore size contrarily to the usual procedure. Values obtained by BJH method and by geometric method are in good agreement with TEM imaging.

#### 4. Conclusions

This work shows that it is possible to optimize the synthesis of silica mesoporous thin films to make them compatible with the use of a 2024 aluminum substrate. This result is made possible by avoiding calcination treatment and by using, as an alternative, UV/ozone illumination to remove the templating agent from the film at room temperature. Mechanical tests have indeed shown that the treatment based on UV did not impact mechanical properties of 2024 aluminum. The oxidization of the substrate due to UV/O<sub>3</sub> treatment and evidenced by EIS measurements on bare aluminum is also avoided when sol-gel film is applied on aluminum. The removal of the Pluronic P123 from the film was shown by FTIR analyses. Furthermore, the treatment provides mesoporous film presenting high pore volume and high specific surface area, as demonstrated by TEM imaging and adsorption porosimetry. It was also shown by EIS measurements that pores are interconnected and form pathways open on the aluminum surface.

The mesoporous thin film, as synthesized in this work, will be loaded with corrosion inhibitors and will constitute the first layer of a protective coating regarding the replacement of chromates based surface treatment. For the further step of incorporation of corrosion inhibitors inside mesopores, the film characteristics determined in this work are very promising. Corrosion inhibitors could be added in the film close to the metallic surface, promoting the healing of the aluminum surface in case of corrosion processes.

#### Acknowledgements

Isaline Recloux wishes to thank the FRIA (Fonds pour la Formation à la Recherche dans l'Industrie et l'Agriculture) for funding. This study was also done in the framework of the Opti2mat "Programme Excellence" financed by the Walloon Region (Belgium).

TGA measurements were performed by F. Khelifa in the "Matériaux Polymères et Composites" department of University of Mons (BE). Authors also would like to thank the "Laboratoire Interfaces et Fluides complexes" from University of Mons (BE) for the use of the UV-ozone cabinet, the "Metallurgie" department for the use of nanoindenter and finally the Sonaca for providing aluminum.

#### References

- [1] J. Dewalque, R. Cloots, F. Mathis, O. Dubreuil, N. Krins, C. Henrist, *Journal of Materials Chemistry* 21 (2011) 7356.
- [2] I. Izquiedo-Barba, M. Vallet-Regi, N. Kupferschmidt, O. Terasaki, A. Schmidtchen, M. Malmsten, *Biomaterials* 30 (2009) 5729.
- [3] A. Bearzotti, J.M. Bertolo, P. Innocenzi, P. Falcaro, E. Traversa, *Journal of the European Ceramic Society* 24 (2004) 1969–1972.
- [4] P.C.A. Alberius, K.L. Frindell, R.C. Hayward, E.J. Kramer, G.D. Stucky, B.F. Chmelka, *Chemistry of Materials* 14 (2002) 3284–3294.
- [5] G.J.A.A. Soler-Illia, P. Innocenzi, *Chemistry: A European Journal* 12 (2006) 4478–4494.
- [6] M.P. Tate, B.W. Eggiman, J.D. Kowalski, H.W. Hillhouse, *Langmuir* 21 (2005) 10112–10118.
- [7] L.C. Huang, E.K. Richman, B.L. Kirsch, S.H. Tolbert, *Microporous and Mesoporous Materials* 96 (2006) 341–349.
- [8] D. Grosso, F. Cagnol, G.J.A.A. Soler-Illia, E.L.C. Crepaldi, H. Amenitsch, A. Brunet-Bruneau, A. Bourgeois, C. Sanchez, *Advanced Functional Materials* 14 (2004) 309–322.
- [9] L. Pei, K. Kurumada, M. Tanigaki, M. Hiro, K. Susa, *Journal of Colloid and Interface Science* 284 (2005) 222–227.
- [10] Z.-L. Hua, J.-L. Shi, L. Wang, W.-H. Zhang, *Journal of Non-Crystalline Solids* 292 (2001) 177–183.
- [11] I. Mukherjee, J. Chen, H. Yin, Y. Wei, *Powder Technology* 206 (2011) 214–217.
- [12] M. Keene, R. Denoyel, P. Llewellyn, *Chemical Communications* 20 (1998) 2203–2204.
- [13] S.V. Lamaka, M.L. Zheludkevich, K.A. Yasakau, R. Serra, S.K. Poznyack, M.G.S. Ferreira, *Progress in Organic Coatings* 58 (2007) 127–135.
- [14] S.V. Lamaka, M.L. Zheludkevich, K.A. Yasakau, M.F. Montemor, P. Cecilio, M.G.S. Ferreira, *Electrochemistry Communications* 8 (2006) 421–428.
- [15] E.V. Skorb, D. Fix, D.V. Andreeva, H. Möhwald, D.G. Shchukin, *Advanced Functional Materials* 19 (2009) 2373–2379.
- [16] J.G. Kaufman, *Properties of Aluminum Alloys, Tensile, Creep and Fatigue Data at High and Low Temperatures*, ASM International, 1999, pp. 1–317.
- [17] F. Cagnol, D. Grosso, G.J.A.A. Soler-Illia, *Journal of Materials Chemistry* 13 (2003) 61–66.
- [18] A. Franquet, H. Terryn, J. Vereecken, *Surface and Interface Analysis* 36 (2004) 681–684.
- [19] M. Baklanov, L. Vasilyeva, T. Gavrilova, F. Dultsev, K. Mogilnikov, L. Nenasheva, *Thin Solid Films* 171 (1989) 43–52.
- [20] C. Boissière, D. Grosso, S. Lepoutre, L. Nicole, A. Brunet Bruneau, C. Sanchez, *Langmuir* 21 (2005) 12362–12371.
- [21] M. Textor, R. Grauer, *Corrosion Science* 23 (1983) 41–53.
- [22] A. Franquet, C. Le Pen, H. Terryn, J. Vereecken, *Electrochimica Acta* 48 (2003) 1245–1255.
- [23] J.A. Gonzalez, V. Lopez, A. Bautista, E. Otero, X.R. Nova, *Journal of Applied Electrochemistry* 29 (1999) 229.
- [24] S.G. Mazzini, J.C. Caretti, *Scripta Metallurgica et Materialia* 25 (1991) 1987–1990.
- [25] P. Falcaro, D. Grosso, H. Amenitsch, P. Innocenzi, *Journal of Physical Chemistry* 108 (2004) 10942–10948.
- [26] C.J. Brinker, Y. Lu, A. Sellinger, H. Fan, *Advanced Materials* 11 (1999) 579–585.
- [27] Q. Huo, D.I. Margolese, U. Ciesla, D.G. Demuth, P. Feng, T.E. Gier, P. Sieger, A. Firouzi, B.F. Chmelka, F. Schuth, G.D. Stucky, *Chemistry of Materials* 6 (1994) 1176–1191.
- [28] G. Sauerbrey, *Zeitschrift für Physik* 155 (1959) 206.
- [29] R.A. Pierotti, J. Rouquerol, *Pure and Applied Chemistry* 57 (1985) 604–619.
- [30] M.R. Baklanov, K.P. Mogilnikov, V.G. Polovinkin, F.N. Dultsev, *Journal of Vacuum Science & Technology* 18 (2000) 1385–1391.
- [31] S. Brunauer, P. Emmett, E. Teller, *Journal of the American Chemical Society* 60 (1938) 309–319.